DEVELOPMENT OF PHOTOCHEMICAL ETCHING AND ITS APPLICATION IN FABRICATION OF INTEGRATED REFLECTOR METAL-SEMICONDUCTOR-METAL PHOTODETECTORS

BY

ADITI UDUPA

THESIS

Submitted in partial fulfillment of the requirements
for the degree of Master of Science in Electrical and Computer Engineering
in the Graduate College of the
University of Illinois at Urbana-Champaign, 2017

Urbana, Illinois

Adviser:

Professor Lynford Goddard

ABSTRACT

Photolithography and etching form the basis of any microfabrication process. Consequently, there is a lot of interest in the research community to improve and innovate on these crucial steps so as to realize the fabrication of complex devices. Once limited to use as physical photomasks for producing planar features, photolithography and etching are now being expanded to function with virtual programmable masks and to produce complex non-planar structures. These "3-D" structures are of great interest in fields like photonics, microfluidics and microelectromechanical systems (MEMS). A number of competitive solutions have been proposed to enable this "grayscale" processing of materials.

This thesis discusses digital projection photochemical etching as a possible tool for maskless, grayscale lithography and etching in a single step. It is based on light-assisted etching of semiconductors placed in a suitable chemical solution. By projecting spatially varying intensity light, grayscale etching can be achieved. The thesis begins with the motivation and literature review of this area of study, and then discusses the fundamental mechanisms of the photochemical etching process. Finally, an application of the fabrication of high-responsivity metal-semiconductor-metal (MSM) photodetectors is discussed to show how photochemical etching can be integrated with conventional microfabrication to enhance device fabrication capability.

ACKNOWLEDGMENTS

I would like to thank my advisor, Professor Lynford Goddard, for his guidance and support through the course of this project and for his resourceful suggestions. I would like to acknowledge the invaluable help I received from Dr. Xin Yu, especially for his advice related to device fabrication. I would like to thank other members of the Photonics Systems Laboratory for their help in this project.

I would like to thank my parents for their constant encouragement and support. Finally, I would like to give special thanks to my friends in Urbana and West Lafayette for their unconditional love and care. This work was supported in part by a grant from the National Science Foundation (ECCS-1509609).

TABLE OF CONTENTS

CHAPTER 1

INTRODUCTION

1.1 Motivation

With semiconductor devices becoming ubiquitous, microfabrication processes have had to keep up with the latest demand and standards of devices. Although microfabrication of silicon microelectronic devices has been well-established in the past 40 years, devices in photonics, microfluidics and micro-electro-mechanical systems (MEMS) require new process tools that are currently being perfected. These new application areas of semiconductors require different materials like III-V semiconductors whose physics and chemistry are inherently different from those of silicon.

Further, because many of these devices are essentially microscale versions of macro-devices like lenses, mirrors, and gratings, they require a non-planar processing capability that conventional silicon microfabrication does not afford. Photolithography and etching, which are the two key steps in any microfabrication process, are essentially binary in nature. Existing technologies to expand photolithography and etching for grayscale topographies are either expensive or labor-intensive. These will be reviewed in the next section. Digital projection photochemical etching presents a solution to this need for grayscale etching, which is cost-effective and simple.

1.2 Literature review

The idea of etching grayscale topographies has been pursued by several groups. The most common method for achieving grayscale etching is to use grayscale photomasks where the intensity of light transmitted varies spatially. This can be done through varying the ratio of opaque to transparent

pixels or through high-energy beam sensitive (HEBS) grayscale masks. A digital mirror device (DMD) has been used in [1] to expose submicron features on the photoresist. In [2], a microstereolithography approach has been used to deposit layer by layer of material. In [3], they use electron-beam (e-beam) to masklessly expose grayscale patterns onto the resist.

Photochemical etching (PC) is a light-assisted etching process. By using inert chemicals, which do not etch the substrate in the dark, maskless lithography and etching can be combined into one single step. Towards this end, there have been efforts for decades to realize photochemical etching on different materials. The author in [4] provides a review of the mechanism and physics of PC etching from a band-bending perspective. There have been several fundamental studies on the parametric dependence of PC etching. A detailed study is presented in [5] of the hole transport equations and the effects of parameters like reaction velocity, diffusion length, absorption coefficient and space-charge width in determining the resolution of a PC etching process for making sinusoidal gratings. In [6], the dependence of InP's etch rate on temperature and pulsed illumination was studied. They found that the etch rate increases linearly with intensity before it saturates, and that it increases almost exponentially with temperature due to the etch being reaction-limited. PC etching, unlike wet etching, has a unique dependence on the doping of the semiconductor. In general, p-type materials do not PC etch whereas n-type materials do. In [7], they ascribe it to the opposite type of band-bending seen at the semiconductor-electrolyte interface. They use deep UV light of 257 nm to generate using "hot holes" and show that n, p and intrinsic GaAs can be PC etched in this technique. In [8], they tackle the same problem by trying to apply a pulsed potential between the p-type GaAs and electrolyte, to PC etch it in a reductive way. In [9], this dopant-dependent PC etching has been leveraged to selectively etch GaAs homostructures.

Apart from the intensity and doping dependence, PC etching also presents the possibility for anisotropic wet etching. In [10], highly anisotropic wet etching of n-type GaN was demonstrated by using uniform UV illumination over a masked sample. PC etching also depends on the purity of crystals and dislocation densities. Dislocation densities were accurately predicted by PC etching n-type GaN by corresponding it to the formation of etch pits. In some regimes, the authors of [11] observed the formation of GaN whiskers,

which they ascribe to threading dislocations in the substrate.

1.3 Outline of thesis

In this thesis, the simplicity and uniqueness of digital projection photochemical etching will be leveraged both for increasing fundamental understanding about PC etching as well as for device fabrication. Unlike work in the literature where illumination is through a focused laser beam or through flood illumination on a patterned sample, the digital projection technique represents an integrated maskless lithographic and etching process.

Firstly, the background of PC etching will be presented by developing its two major components: wet etching and semiconductor band-bending. Next, the details of the optical setup will be presented along with specifications of the experimental procedure. Further, the results of several PC etching experiments to study its anisotropy, defect-dependence, and diffusion-limitedness will be presented. Next, the use of PC etching in the fabrication of metal-semiconductor-metal photodetectors (MSM-PD) will be outlined with some preliminary results. Some limitations and outlooks for the future will be discussed in the conclusion.

CHAPTER 2

BASICS OF PHOTOCHEMICAL ETCHING

2.1 Mechanism of semiconductor wet etching

Fabrication of a semiconductor device involves several processing steps in order to achieve the desired electrical and optical properties. Some common steps are photolithography, etching and metallization. Metallization is usually the final step of the process where electrical contacts are laid out for injecting current. Photolithography is used to define patterns on a substrate by using photoresist as masks. Etching is a step succeeding photolithography where the unmasked regions of the material are subject to material removal, thereby creating binary 3D patterns.

Etching is an essential step in almost all device fabrication processes. There are several reasons for etching material. Some examples are:

- To remove surface damage and reveal polished surfaces
- To reach to an underlying layer beneath the top layer, for making contacts
- To create electrical isolation between parts of the substrate by forming mesa structures
- To create channels for light in optoelectronics like microrings, waveguides and so on

Wet etching is when liquid solutions (etchants) are used to remove material. The etchant is chosen such that it only attacks the unmasked regions while remaining almost inert to the masking material. It occurs by chemical reactions at the surface. *Dry etching* is when material is removed both through physical bombardment of ions and through chemical corrosion. Table 2.1 compares the characteristics of these two methods.

Table 2.1: Comparison of Wet and Dry Etching

Feature	Wet etching	Dry Etching
Mechanism	Chemical	Physical and chemical
Directionality	Isotropic	Anisotropic
Selectivity	High	Low
Quality of surface	Smooth	Can have rough sidewalls

Wet etching is low-cost and highly selective, but suffers in its isotropicity and inability to etch small features. Therefore, an anisotropic wet etch process is highly desirable. Wet etching proceeds through the following series of steps:

1. Diffusion of the etchant molecule to the surface
2. Chemical reaction of the etchant molecule and surface molecule to form a soluble product
3. Diffusion of the reaction products away from the surface to reveal new material

The etching process, therefore, may be limited by either the diffusion processes or the chemical reaction process. If the rate at which reactants and products are transported is much slower than the chemical reaction, it is called *diffusion-limited* etching. If the rate at which the chemical reaction occurs is much slower than the transport, it is called *reaction-limited* etching. The regime of etching depends on the chemical composition, agitation of the etchant, temperature, and the substrate itself. Each regime has its own uses.

Diffusion-limited etching is more isotropic producing rounded and polished edges. The mask edges show enhanced etching (called trenching). It is highly sensitive to agitation/stirring and viscosity of the etchant, but not so much to temperature.

Reaction-limited etching is selective to crystalline facets and can be highly anisotropic. It is sensitive to temperature but not so much to agitation of the etchant.

The general mechanism of wet etching applies to GaAs (which we mostly worked with). However, more can be said regarding the etchants of GaAs. Almost all of them start off by oxidizing the surface to form gallium oxide and arsenic oxide. These oxides are then dissolved by a complexing agent

like an acid or base. One common etchant (solvent/oxidizer/medium) is $H_2SO_4/H_2O_2/H_2O$. Both the oxidizer and solvent are needed for etching GaAs. Other examples are $HCl/H_2O_2/H_2O$, $H_3PO_4/H_2O_2/H_2O$, bromine-methanol and so on. The etch rate is mostly decided by the concentration of the oxidizing agent and can be as high as 1-2 μm/min. Etch rate increases with temperature (for reaction-limited) and with agitation (for diffusion-limited). It is observed that slow etching tends to produce smoother surfaces.

2.2 Band-bending at the semiconductor-electrolyte interface

General wet etching is mostly just a chemical corrosion of material by the etchant. Photochemical etching, however, depends on the semiconducting properties of the material to be etched. Here, charge carriers like electrons and holes are significant to the etching process. The motion of these charge carriers is guided by the electrochemical potential and hence we will first consider the nature of the potential in a semiconductor-etchant interface. Because this process also involves exchange of ions, the etchant may also be referred to as an electrolyte.

2.2.1 Thermodynamic equilibrium of contacting bodies

When two bodies capable of exchanging charge carriers come into contact, the carriers adjust in such a way that there is no current flow at thermodynamic equilibrium. In other words, the electrochemical potential equalizes in all parts, without any gradients. The electrochemical potential of a system is also called its Fermi level. Hence, when two bodies come into thermal equilibrium, their Fermi levels equalize.

The familiar example would be that of a pn-junction. The Fermi level of n-type material lies close to the conduction band, whereas it lies close to the valence band for a p-type material. When they come into contact, the Fermi levels of both equalize leading to the well-known built-in potential.

2.2.2 Band-bending at interfaces

Now let us consider what physically happens at the interface when the Fermi levels equalize. Since the n-type material has excess electrons compared to the p-type material, electrons near to the interface region flow across. So, the conduction-band bends upwards in the n-type region and downwards in the p-type region. This band-bending is shown in Fig. 2.1. Now consider

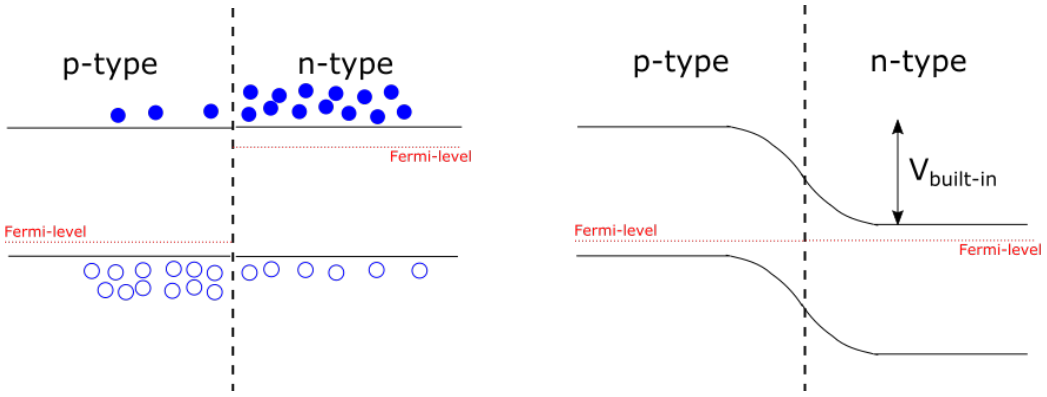

(a) pn-junction before thermal equilibrium

(b) pn-junction after thermal equilibrium

Figure 2.1: Band-bending at p-n semiconductor interface

our case of the interface between a semiconductor and an electrolyte. For an n-doped material/electrolyte interface, similar to the case of pn-junctions, upon equalization of the Fermi levels, the bands bend upwards. This is because electrons go from the semiconductor to the electrolyte by means of a redox reaction. For a p-doped material/electrolyte interface, the bands bend downwards. Figure 2.2 shows the band-bending for the two types of doping.

This band-bending trend is not always the case because it depends on the position of the electrolyte's work function (or Fermi level) with respect to the semiconductor's. But, generally, this is what has been observed.

2.3 Process of photochemical etching

Photochemical etching occurs because of a combination of semiconductor band-bending and wet etching. Let us look at the process for an n-type semiconductor with band-gap E_g. The process can be described by the following sequence of steps, which are illustrated in Fig. 2.3:

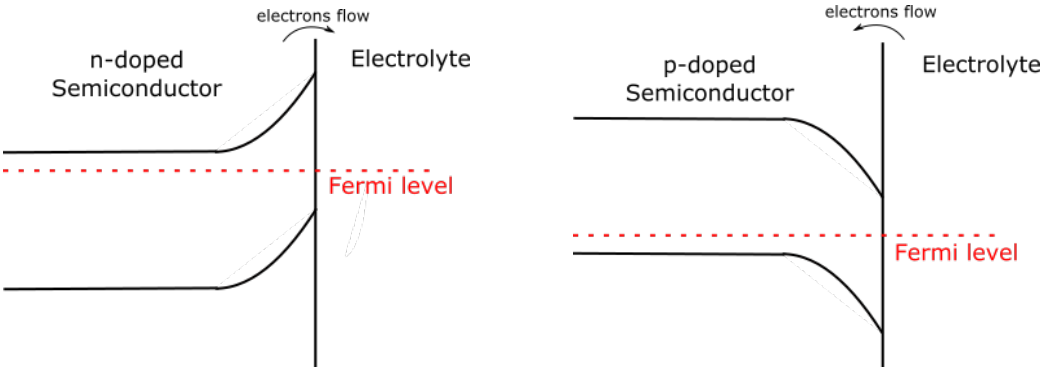

(a) n-type band bending

(b) p-type band bending

Figure 2.2: Band-bending at semiconductor-electrolyte interface

1. Incident photons of energy greater than E_g create electron-hole pairs. The position of the creation of the electron-hole pairs depends on the absorption coefficient of the material for that wavelength.

2. Because the valence band bends upwards near the surface, the photogenerated holes drift to the surface, whereas the photogenerated electrons drift to the bulk.

3. These holes cause redox reactions and lead to oxidation of the surface to form oxides of the semiconductor.

4. The etchant then dissolves these oxides by forming complexes.

This results in etching of material in illuminated regions. As discussed before, wet etching of GaAs occurs by one component of the etchant oxidizing the surface and another component dissolving the oxide. In photochemical etching, the same process occurs but the oxide is formed due to photogenerated holes at the surface. The specific reactions are important to understand as they determine the etching process. For the case of n-type GaAs, they are:

$$\mathrm{e_{VB}} \xrightarrow{\mathrm{h}\nu} \mathrm{e_{CB}} + \mathrm{h_{VB}}$$
$$\mathrm{GaAs} + 6\,\mathrm{h}^+ \xrightarrow{\text{acidic}} \mathrm{Ga}^{3+} + \mathrm{As}^{3+}$$

Basically, there are four mechanisms for motion of holes:

1. Generation - Light is absorbed and holes are generated near to the surface.

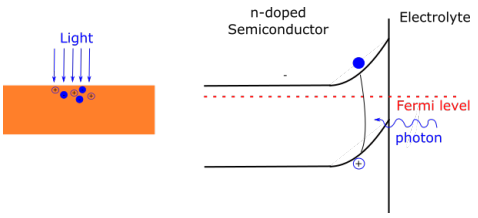

(a) Creation of electron-hole pairs by light

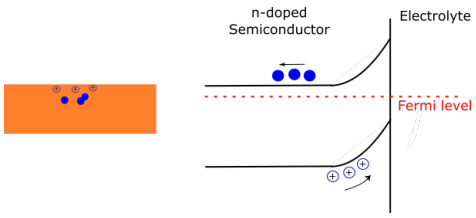

(b) Drifing of holes to the surface

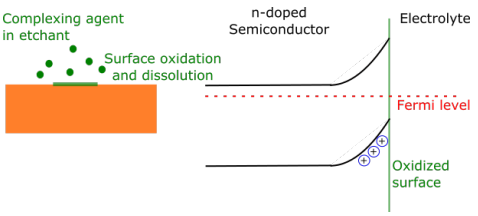

(c) Oxidation of the surface and dissolution

(d) Resulting etched surface

Figure 2.3: Photochemical etching process

2. Drift - The holes move from the bulk to the surface because of the potential gradient in the valence band.

3. Reaction - The holes at the surface react with the GaAs molecules to oxidize the GaAs surface.

4. Diffusion - The holes move from the illuminated region (where they are in high concentration) to the dark region (where they are in lower concentration) due to the concentration gradient. This results in lateral etching.

2.4 Implications

With the physical understanding of the photochemical etching process, it is possible to understand its dependence on parameters and their implications.

2.4.1 Band-gap dependent etching

Only light of energy greater than the band-gap can create electron-hole pairs. Therefore a band-gap dependence of etching is seen, which is not possible in conventional wet etching. Some of the possibilities it presents are:

- creating perfect etch stop layers in multi-layer devices
- creating suspended structures where the material beneath has a lower band-gap than the upper one and can be photochemically etched

2.4.2 Doping dependent etching

As discussed above, for GaAs whose wet etching occurs through oxidation and dissolution, only n-type GaAs can be photochemically etched because of the upward band-bending. In p-type GaAs, electrons drift to the surface and cause reduction of the surface atoms. If there were a chemical that could dissolve reduced products, p-type GaAs could also be etched photochemically. But, we are currently unaware of such a chemical. However, photochemical etching can be used in addition to wet etching as follows. If the chemical we use were to contain an oxidizer (like H_2O_2), it would etch GaAs even without light. The light can, however, increase or decrease the etch rate.

- In the case of n-type GaAs, the illuminated region has oxidation from two sources - the oxidizer and the photogenerated holes. So, it etches faster than the dark regions.
- In the case of p-type GaAs, the illuminated region has a lower oxidation probability because of the competing reduction by the photogenerated electrons. So, it etches slower than the dark regions.

Figure 2.4 shows the optical profiler scan of two etched patterns in n-type and p-type GaAs. The illuminated pattern on both of these was the same 500 μm blue square. The resulting patterns confirm the predictions discussed above. The details of the experimental setup will be discussed in chapter 3.

2.4.3 Intensity dependent etching

The intensity of the light determines the number of electron-hole pairs that are created. So, more intense light creates more surface holes, which yields a higher etching rate. So, by projecting intensity gradient patterns of light onto the sample, gradient structures can be photochemically etched. Figure 2.5 shows the profile of an etched pattern created by using a linear gradient shown in the inset.

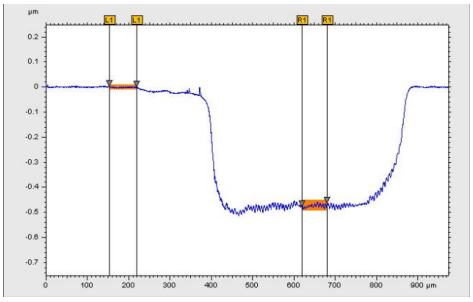

(a) Formation of an etch pit in n-type GaAs because light favors etching. Etchant composition was 3mL HCl + 100mL H_2O and the etching was done for 5 minutes.

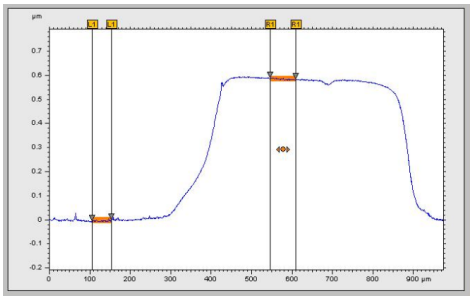

(b) Formation of a mesa structure in p-type GaAs because light hinders etching in the case of p-type GaAs. Etchant composition was 2mL HCl + 2mL H_2O_2 + 200mL H_2O and the etching was done for 30 minutes.

Figure 2.4: GaAs photochemical etching for opposite doping types

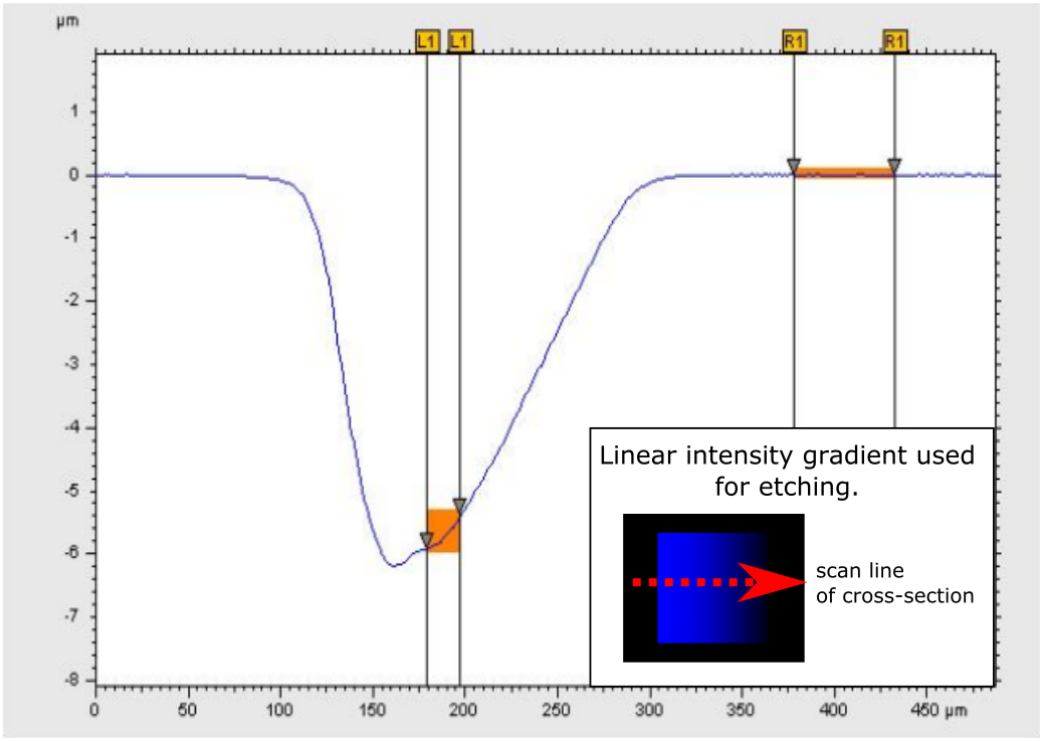

Figure 2.5: Optical profiler scan of an etched sawtooth pattern using the linear-gradient intensity light shown in the inset. The cross-section of the scan is shown as the dotted red line in the inset.

Further applications of the gradient etching will be discussed in chapter 6 and chapter 7. Intensity-dependent etching has great potential to replace the current long-drawn grayscale lithography techniques in a number of applications in photonics, microfluidics, and MEMS.

2.4.4 Crystal defect dependent etching

Because the photochemical etching process depends on the creation of electron-hole pairs, it must have some dependence on defect levels in the crystal. The presence of defects can lead to the recombination of these electron-hole pairs, thereby causing no photochemical etching. So, if we compare two regions, one with crystal defects and one without, the former will etch slower than the latter. This has been observed as etch hillocks on the surface. However, etch pits have also been seen, suggesting that these defect sites may also have enhanced photochemical etching in some cases, due to them being electrically active. Different types of observed defects will be discussed in section 4.3.

CHAPTER 3

EXPERIMENTAL SETUP

3.1 Setup schematic

Figure 3.1 shows the schematic of the optical setup used for photochemical etching. All lenses have a 2 inch diameter.

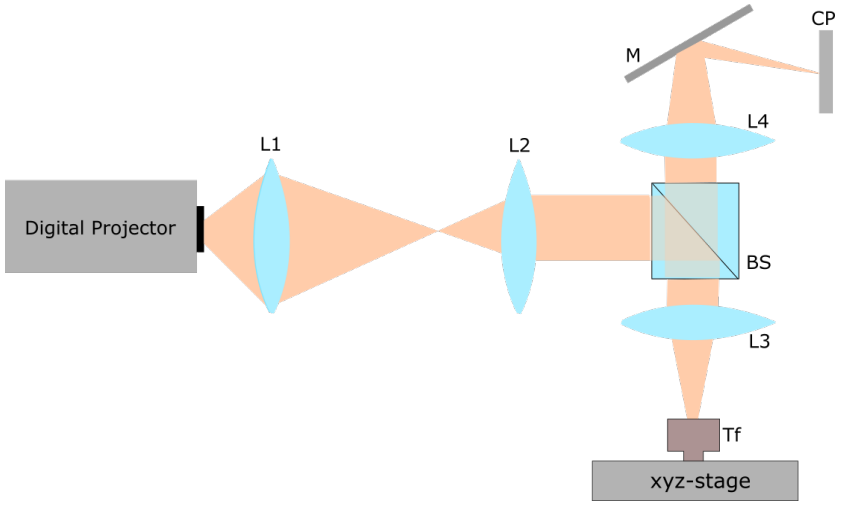

Figure 3.1: Schematic of the photochemical optical setup. L1-4:lenses, BS: beamsplitter, Tf: Teflon cup, M: mirror, CP: conjugate plane.

The pattern to be etched is projected using a ViewSonic PJD7820HD digital projector connected to a computer. First, the diverging beam of the projector is passed through lens L1 to capture all the light before it diverges too much. L1 has a focal length of 75 mm. It forms an image at an intermediate plane between L1 and L2. There is a 4f-system formed by lenses L2 and L3 of focal lengths 300 mm and 75 mm, respectively. The beam is collimated after passing through L2 and about half of the power passes through the beam splitter to lens L3, which is the objective lens. The de-magnified image is then projected onto the sample for photochemical

etching. The magnification ratio from the intermediate plane to the sample plane can be calculated as follows:

$$|m_2| = f_2/f_1 = 75/300 = 0.25$$

So the magnification is 0.25. The sample is placed on an automated Thorlabs PT3 xyz-translation stage with ZST225B actuators. The stage has a positional repeatability relative to a fixed home location of 5 μm and a theoretical minimum incremental motion of 0.5 nm. We adjust the z-knob to bring the sample into focus in the sample plane. To be able to view whether the sample is indeed in the sample plane, we use the concept of the conjugate plane. Because the samples are usually highly reflective ($\approx$ 30%), there is sufficient reflected light that returns through the beam splitter. Half of the reflected power goes vertically to lens L4, which is a 400 mm converging lens. It forms an image of the sample plane 400 mm away. The magnification of this second 4f-system is $\frac{400}{75} \approx 5$. At this conjugate plane, we either place a screen or a camera for better resolution alignment. One pixel on the computer screen of resolution 1920 x 1080 results in 10.52 μm on the sample plane and 56 μm on the conjugate plane. The etching resolution, which is currently limited by the pixel size in the sample plane, can be improved by using a higher numerical aperture (NA) objective lens.

3.2 Steps of photochemical etching

The general steps for the experiment are:

- Sample preparation: The n-type GaAs pieces are cleaved in the cleanroom with a cleaving board under a fume hood. Wearing personal protective equipment (PPE) like nose-mask and goggles is necessary to avoid exposure to the fine dust particles of GaAs, which are toxic. The samples are then cleaned with the standard degreasing step - acetone, isopropyl alcohol (IPA), deionized (DI) water, and IPA. They are dried with a N_2 gun.

- Etchant preparation: The etchants are mixed with the chemicals in the General Chemistry laboratory in the cleanroom under a fume hood.

Some of the general etchants that were used are summarized in Table 3.1.

Table 3.1: Common etchants used for PC etching

Etchant	Composition (mL)	Comments
$HCl:H_2O$	2:100	Slow and smooth etching, dark etch rate is nearly zero
$HCl:H_2O_2:H_2O$	2:0.5:100	Slow etching, generally smooth
$HCl:H_2O_2:H_2O$	2:2:100	Fast etching, sometimes produces needle-like roughness features
$H_2SO_4:H_2O_2:H_2O$	4:1:80	Standard for wet etching, smooth wet etchant, can produce roughness during PC etching

- Pattern preparation: The pattern to be projected on the sample needs to be created in a drawing program such as Microsoft PowerPoint on a computer connected to the projector. The images were generally placed on a black background and they were aligned to the center of the screen. Generally, we used Blue 255 for the color of the pattern. But, when higher etching rates were needed, white was used.
- The sample was placed at the center of the custom Teflon holder shown in Fig. 3.2. The Teflon cup is resistant to attack by most chemicals and it has a flat base. We first filled the cup with 7 mL of water and placed it underneath the objective lens on the xyz stage. The z-knob was adjusted to get the pattern in focus on the sample, by gauging the image on the conjugate plane.

Figure 3.2: The custom-made, acid-resistant Teflon cup

- The Teflon cup with the sample was then drained and re-filled with 7 mL of the etchant. It was quickly placed underneath the objective to begin the etching process. The etch was generally timed to etch to a desired depth. For large etch depths, the sample was translated upwards every few minutes to bring it back into focus.
- After etching, the sample was cleaned with water and dried and the etchant was disposed. As this is done in the general lab outside the cleanroom, we used a compressed air can for drying the sample.
- The most common method used for metrology was the Alpha-step surface profiler in the cleanroom. The etched features can be scanned to measure the etch depth and surface smoothness. The optical microscope was used when general surface quality needed to be inspected. In samples where the etch depth was comparable to the lateral dimension of the feature (i.e the *aspect ratio* was comparable to 1), the scanning electron microscope (SEM) was used to observe the cross-section of the sample. For this, the sample needed to be cleaved either manually or using the automated Scriber tool.

3.3 Photochemical etching as maskless lithography

Conventional photolithography is done by exposing UV light onto a photoresist thin film through a quartz mask with chrome features. After the exposure, the sample is dipped in a developer to remove the exposed photoresist (positive lithography) or the unexposed photoresist (negative lithography). This method is fast and simple. However, the process of making the photomasks is time-consuming and expensive. Although the resolution of the light projection system is sub-micron, to make photomasks with submicron features is very expensive. So, generally, photolithography in our cleanroom is performed for features of size greater than 1 μm.

E-beam lithography is a very high-resolution technique that does not involve using physical masks. The masks are designed on a computer and an electron-beam scans and thereby exposes the photoresist as per the computer design to expose it. Features as small as several nanometers can be easily patterned. However, this has not taken a place in industry and is limited to research because of its slow throughput and high cost.

To obtain high resolution with high throughput, several other types of lithography like nano-imprint lithography, optical maskless lithography (direct laser writing) and so on have been developed. There is a strong desire for techniques that use programmable masks.

The subsequent step after photolithography is generally wet or dry etching, using the photoresist as a hard mask. In view of this, photochemical etching can be viewed as a maskless lithography + etching step. By shining light, we automatically mask the dark regions and etch the illuminated regions. Thus, it removes the need for an intermediate lithography step altogether. The challenge would be to obtain good resolution.

Using blue light (λ = 400 nm) and an objective of NA $\approx$1, we can at best get a resolution of 400 nm. However, there are practical challenges. Firstly, the optical setup has many non-idealities like aberrations from lenses, multiple reflections, and other focusing errors, which result in some spread of the projected pattern. Further, the lateral diffusion of electrons and holes leads to etching in regions outside the projected pattern, thereby increasing the feature size. If these challenges can be overcome, photochemical etching can be used as a high-throughput, low-cost, one-step maskless lithography and etching step for semiconductors. Nevertheless, it is a good option for cases with features more than a few microns.

CHAPTER 4

DEVELOPMENT OF PROCESS INSIGHTS

Photochemical etching depends on semiconductor properties and physics more than conventional wet etching does. Generation of electron-hole pairs by light implies that several concepts like diffusion, recombination, and electric field will play a role in photochemical etching. This chapter will cover some of the insights that were developed in the course of performance of several etching experiments.

4.1 Anisotropic wet etching

The main advantage of dry over wet etching is its directionality and consequently its ability to produce nearly vertical sidewalls. This is because the etching is highly anisotropic, with the vertical etch rate being much greater than the lateral etch rate. This anisotropy produces almost no undercut of the mask, thereby preserving the designed feature sizes. It is also essential in cases where the feature lateral size is on the order of the etch depth. Isotropic etching would totally etch away the feature in such a case. Vertical etching is also desirable in the fabrication of photonic devices like waveguides where spurious angles for the waveguide walls may cause uncontrolled modal properties. Dry etching proceeds through a combination of plasma chemical etching and kinetic bombardment by ions. The latter is responsible for the anisotropicity of the dry etching technique. For GaAs especially, dry etching remains the only method for producing vertical sidewalls as even rate-limited wet etching cannot produce 90^0 sidewalls.

Wet etching has almost equal etch rate in all directions and produces mask undercuts as shown in Fig. 4.1. The mask in the figure is a 7μm ridge with layers as shown in Fig. 4.2.

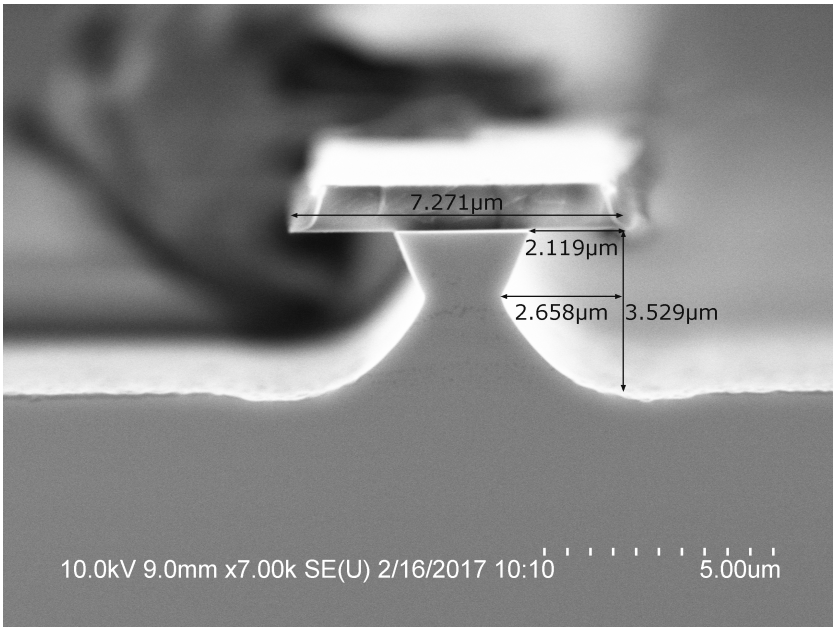

Figure 4.1: Cross-section SEM of sample after 60 min wet etching with 4:1:80 H_2SO_4:H_2O_2:H_2O

Wet etching, however, presents several other advantages. Apart from the simpler equipment and lower cost, it has high selectivity with respect to different materials and can produce smooth sidewalls. It can also provide faster etch rates compared to dry etching. Therefore, an anisotropic wet etch is highly desirable.

Photochemical etching relies on wet etching via creation of light-generated electron-hole pairs. Because the carriers are produced only in the illuminated regions, the etching should take place only vertically in principle because the sidewalls are not illuminated. There are some practical issues, however, to be considered. Firstly, the illuminated surface may not be perfectly perpendicular to the light or the surface may not be perfectly flat, and so some portion of the light may reflect onto the sidewalls causing them to etch. Further, the light-generated charge carriers diffuse laterally onto the dark regions because of the concentration gradient created. Hence, a region around the illuminated region also undergoes PC etching. Nevertheless, the lateral etching is small compared to the vertical etching and hence anisotropicity can be expected.

To compare the anisotropy between wet and PC etching, an n-type GaAs sample was patterned with 83 μm metal mask to open a circular window with a half-bridge. The side-view schematic is shown in Fig. 4.2.

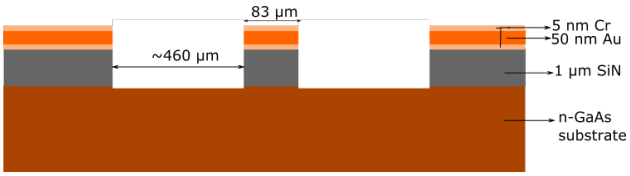

Figure 4.2: Schematic of the cross-section of the sample across the half-bridge, showing the various layers making up the hard mask

This sample was then used for PC etching by projecting a white circle to overlap with the open area of the sample. Etching was done for 20 minutes with a 4:1:80 H_2SO_4:H_2O_2:H_2O solution. The sample was seen to etch close to 90 μm deep. Another sample patterned with 100 μm wide ridges of the same masking materials was used for comparing the wet etching anisotropy. To achieve 90 μm etch depth with wet etching with the same etchant would take about 15 hours, which we tried. However the undercut led to stripping of the mask completely. So, we performed the wet etching for just 3 hours to achieve an etch depth of about 18 μm. The SEM images of the two cases are shown in Fig. 4.3.

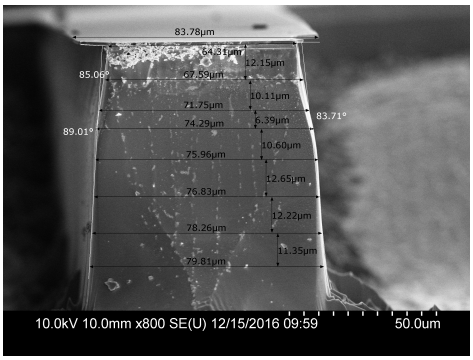

(a) Cross-section SEM of a PC-etched sample

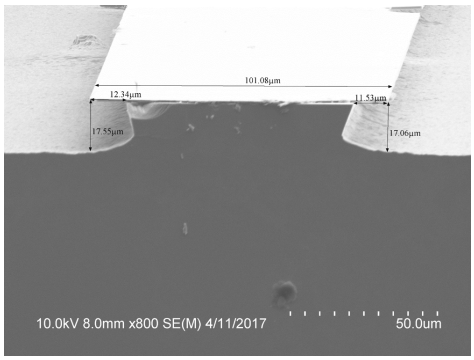

(b) Cross-section SEM of a wet-etched sample

Figure 4.3: Comparison of etching anisotropy for PC and wet etching

The lateral undercut for the PC etch case is 20 μm whereas it is 23 μm for the wet etch case. The anisotropy can be defined as $A = \frac{\text{Vertical etch depth}}{\text{Lateral etch depth}}$. From the SEM images, we can see that $A_{PC} = \frac{90}{20} = 4.5$ whereas $A_{wet} = \frac{18}{23} = 0.8$. So, PC etching can be close to 6 times more anisotropic than wet etching. Further, the angle of the sidewall for the PC etching can be approximately seen to be 86^0. It is to be noted that the etchant used for the PC etching was a wet etchant with an oxidizer so it also has a finite

dark etch rate. Hence, even better results are expected if the etchant for PC etching did not include the oxidizer making the dark etch rate nearly zero. This would decrease the lateral etch rate further.

4.2 Visualization of substrate defects

Crystal defects play an important role in determining electronic and photonic properties of materials like recombination lifetime, mobility, surface quality and so on. Wafers are usually tested for defects and dislocations by means of tools like transmission electron microscopy (TEM), which can be expensive and are time consuming to prepare samples.

An alternate approach has been to use *preferential wet etching* where certain chemical etchants are used to reveal the dislocation structure by means of certain artifacts like etch pits, hillocks and so on. For GaAs, a common preferential etch is the Abrahams-Buiocchi (AB) etch ([12]) where structures like etch pits and lines are seen corresponding to differently oriented dislocations and stacking faults. The main mechanism of this technique is that different faces have different chemical reactivity that sensitive etchants can reveal.

PC etching relies on generation and separation of electron-hole pairs. Naturally, crystal defects will play a role because of the mid-gap trap states that they cause in the band-structure of the crystal. The photogenerated electron-hole pairs get trapped in these states, which occur close to a defect. Thus defect sites would etch differently. Additionally, the defect-sites can have a different distribution of electric field and may attract/repel carriers once again causing it to etch differently. The intricate mechanism of how the defect will affect the photogenerated carriers is quite complex, but it is clear that it should have some effect on the etch quality. This can then be used to empirically determine the substrate quality.

It was particularly noted that etching for a long time or etching at a fast rate tended to produce structures like etch pits and roughness. Three prominent types of defect-related structures were seen during PC etching.

1. Etch pits: Figure 4.4 shows an SEM image of a sample surface after PC etching for 10 minutes with 2:2:100 HCl:H_2O_2:H_2O etchant. The similar orientation of each of the etch pits suggests that it is a result

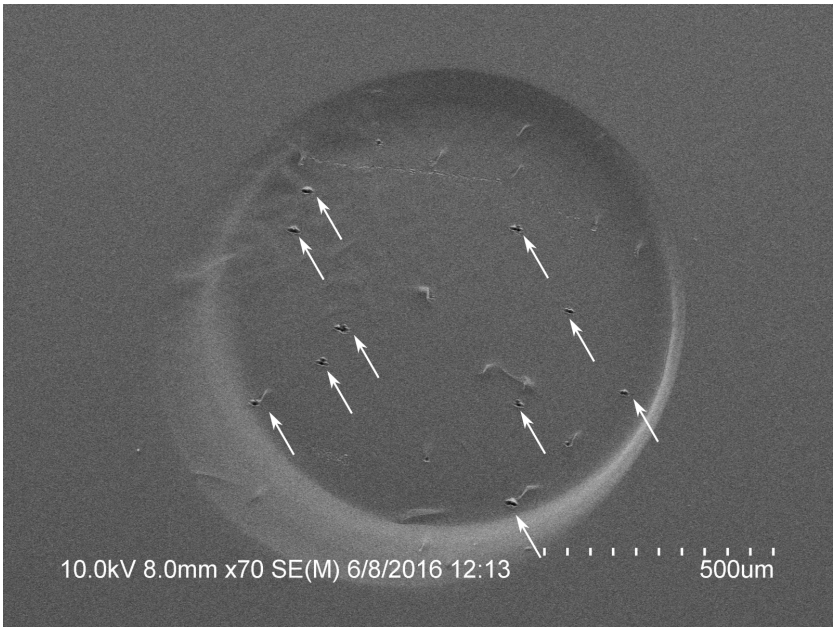

Figure 4.4: Similarly oriented etch pits seen after PC etching

of defect in crystal structure and not merely a product of enhanced etching due to external conditions.

2. Needle structures: Figure 4.5 shows a cross-section SEM image of a sample after PC etching for 83 minutes with 2:0.5:100 HCl:H_2O_2:H_2O etchant. The needle-shaped structures are more than 50 μm long, which suggests that the defects in this case are not localized ones but something that extends into the wafer. One such defect would be a threading dislocation.

3. Octahedral crystal-like residues: Figure 4.6 shows a top-view and Fig. 4.7 shows a side-view of a peculiar type of structure seen after PC etching on a sample. It was not seen in a reproducible way even when the same etchant was used on the same sample. With some experimental trials, it was seen that by first etching with 2:2:100 HCl:H_2O_2:H_2O for 10 minutes, a few defects in the form of etch pits would show up. When this was followed by a long etch (>30 minutes) using 4:1:80 H_2SO_4:H_2O_2:H_2O etchant, such structures were formed more reproducibly (but not with certainty). The structures seem like octahedral crystals placed on volcano-like pits.

   The octahedra residues were tested for composition using the energy

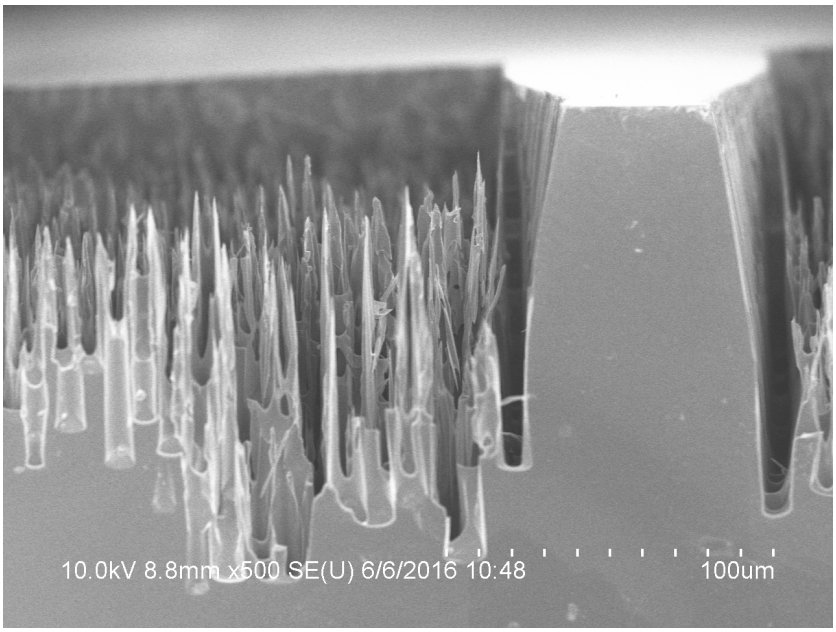

Figure 4.5: Needle-like structures possibly indicate presence of threading dislocations

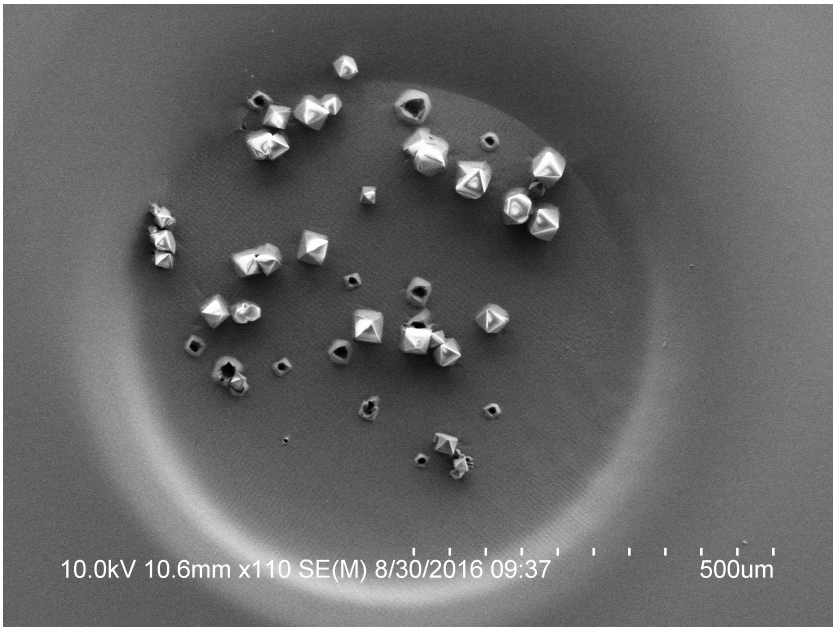

Figure 4.6: Top-view SEM of dispersed octahedral-like structures seen after PC etching a 1mm-radius circle

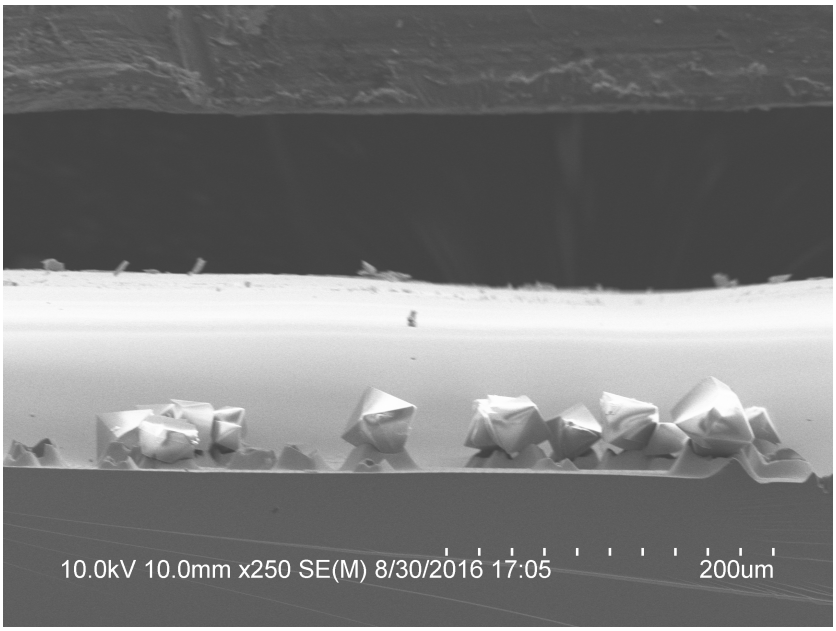

Figure 4.7: Side-view SEM of the octahedral-like structures

dispersive X-Ray spectroscopy (EDS) tool in the Materials Research Laboratory (MRL). The sample is n+-GaAs with silicon doping of 10^{18}cm^{-3}. Figure 4.8 shows the EDS data of the composition of the octahedral-like structures whose SEM can be seen in the inset. Table 4.1 shows the percentage composition of the identified elements in the spectrum.

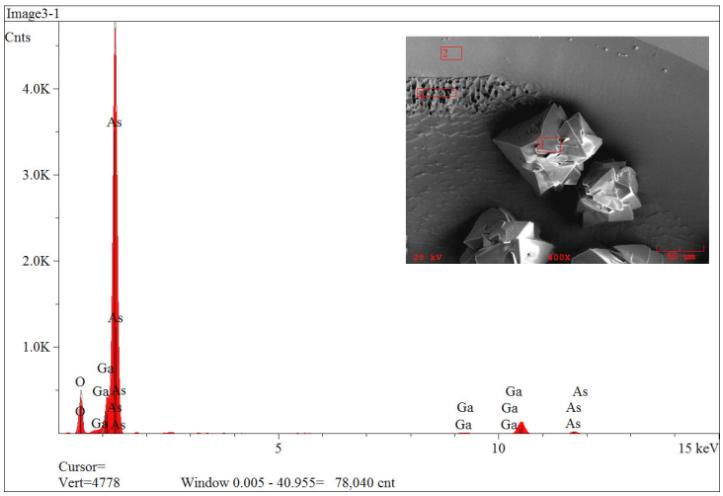

Figure 4.8: EDS data showing peaks at Ga, As and O at the octahedral-like structures (inset)

Table 4.1: Percentage composition of elements in the octahedral-like structures using the EDS spectrum

Element	Percentage (wt%)
Ga	4.6
As	84.9
O	10.5

The presence of O and large quantities of As suggests that the octahedra-like structures are rich in arsenic oxide. One hypothesis is that the gallium oxide and arsenic oxide which form during PC etching have different solubility rates, the arsenic oxide being slower to dissolve accumulates in certain regions. However, the reason behind the formation of these regular clusters is still not understood.

4.3 Diffusion-limited etching

Wet etching can either be diffusion-limited or reaction-limited as discussed previously. One characteristic feature of diffusion-limited etching is trenching at the mask edges. As can be seen in Fig. 4.1, the etch rate at the mask edge is higher than in the center of the window, which shows up as trenching at mask edges. The etchant concentration at the mask edges is lower because the rate of consumption there is higher. In [13], the wet etch process is simulated using a Monte Carlo technique where individual etch events are broken down as: (i) transport of an etchant molecule to the surface, (ii) reaction at the surface, (iii) transport of product away from the surface. The degree of diffusion-limitedness is varied with a parameter γ. For completely diffusion-limited etching, $\gamma = 1$ and the reaction step (ii) occurs instantaneously when the etchant molecule reaches the surface. For completely rate-limited etching, $\gamma = 0$ and the diffusion steps occur instantaneously. The algorithm was implemented using Matlab and Fig. 4.9 compares the simulated etch profile for various values of γ. The more diffusion-limited the reaction, the more trenching seen at the mask edge.

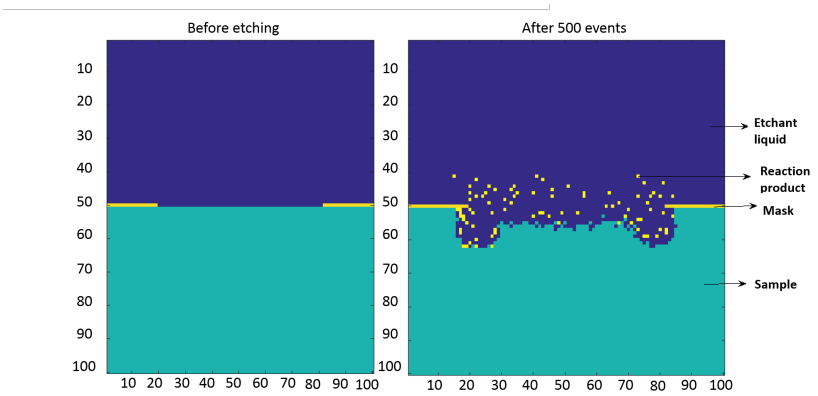

(a) Cross-section before and after 500 etching events

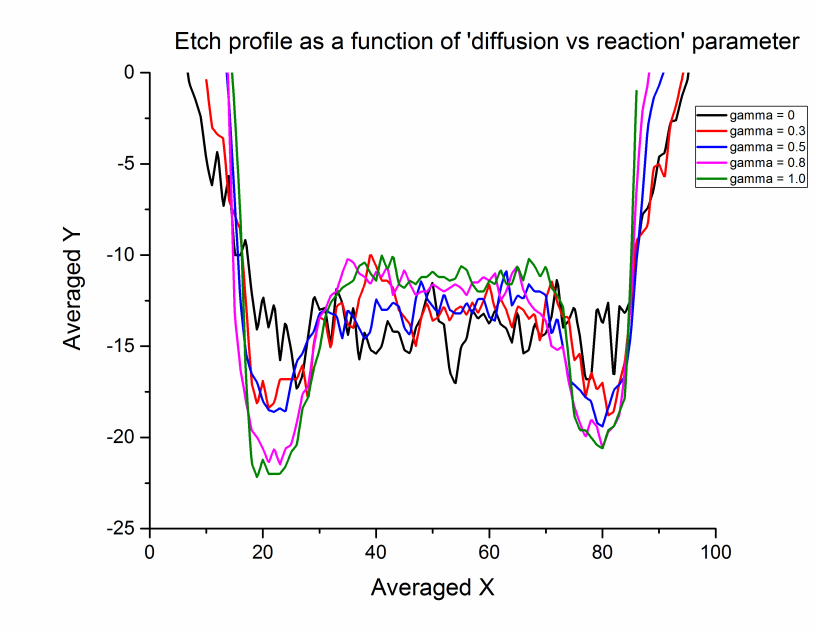

(b) Etch profile for different values of γ

Figure 4.9: Variation of trenching with diffusion-limitedness of the etch process

Because photochemical etching allows us to locally create etchant sinks because of its high etch rate, a spatial variation in etch rate could be created. Figure 4.10 is a schematic of the mask that was used for this experiment. It has several identical open circular shapes of 1 mm diameter with a half-bridge. In one case, the sample was etched in the dark (by projection of a black screen) with 2:2:100 HCl:H_2O_2:H_2O. In the other case, a similarly patterned sample was photochemically etched with the same etchant by pro-

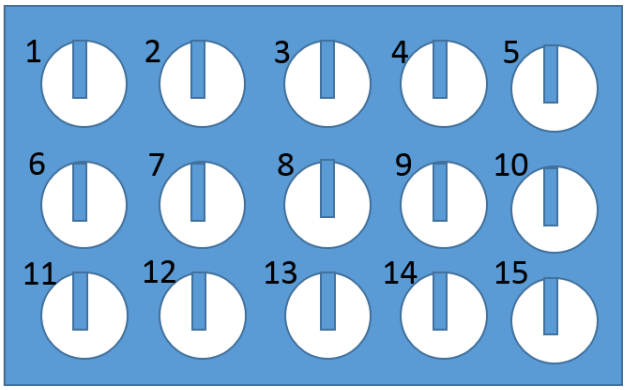

Figure 4.10: Schematic of the mask used. The masked part is shown in blue. It is Si_3N_4. The exposed GaAs part is shown in white.

jecting a white circle on the same black screen, only onto one of the circles. The other circular windows were left in the black screen area. Both samples were etched for 30 minutes. The optical profile scan line is approximately at the center of each circle. Figure 4.11 shows the profiles of the circle marked 7 for the two samples. There is a consistently larger mask-edge trenching seen in the photochemical etching case compared to the pure wet etching case. This can be attributed to the fact that the light creates an etching

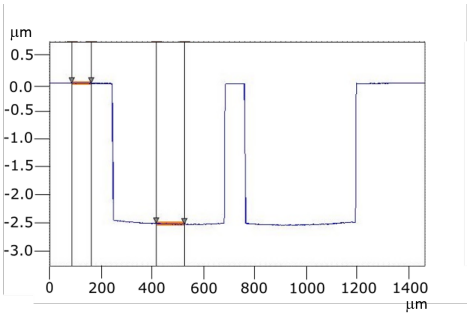

(a) Profile of circle 7 of the sample etched under a black screen

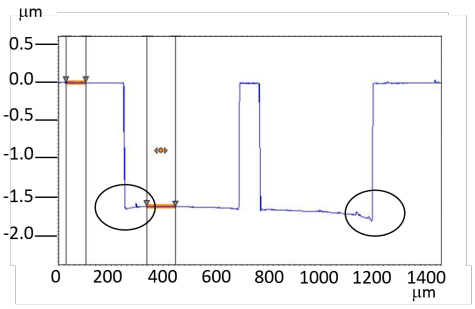

(b) Profile of circle 7 sample etched with an illuminated circle at 8

Figure 4.11: Etch profiles of circle 7 without and with illumination on circle 8. In addition to trenching, the etch depth is smaller in (b) because of the nearby illumination

"hotspot" to which most of the etchants diffuse, making etching in the other circles more diffusion-limited. In other words, the PC etching is an etchant sink and neighboring areas get a smaller influx of etchant molecules.

CHAPTER 5

METAL-SEMICONDUCTOR-METAL PHOTODETECTOR

Photodetectors are an important component of optics and photonics instruments. They are used to detect light and produce a proportional amount of electric signal that can be measured. They are used in conjunction with optical sources like lasers and light-emitting diodes (LEDs). Photodetectors are used for large-area detection as in optical setups and small-area detection in photonic circuits. In optical communication, data is transmitted at high speeds across optical fibers, which then have to be digitally processed. So, the light from the fiber is coupled onto a high-speed photodetector, which produces electric current that can then be digitized and processed.

The general mechanism of photodetection is as follows:

1. Creation of electron-hole pairs by light in a semiconductor
2. Transport of the electron-hole pairs in an electric potential to metal contacts
3. Generation of current due to the motion of charge carriers

For creation of electron-hole pairs by the light, the light has to be absorbed in the semiconductor. Figure 5.1 shows a diagram of absorption coefficient (α) versus the wavelength of light. Most of the materials show a sharp drop in α at a particular wavelength. This occurs at the band-gap wavelength. Light of energy less than the band-gap, i.e. longer wavelength, goes through the semiconductor nearly unabsorbed. Photodetectors cannot be operated efficiently in this regime. Further, the absorption coefficient is also a measure of how deep below the surface the light will typically be absorbed. GaAs has a band-gap of $E_g = 1.424$ eV. So the cut-off wavelength is $\lambda_c = \frac{1240}{E_g} = 870$ nm. Therefore, GaAs photodetectors can be used to detect visible light (400 - 700 nm). Absorption of light is only the first requirement for a photodetector.

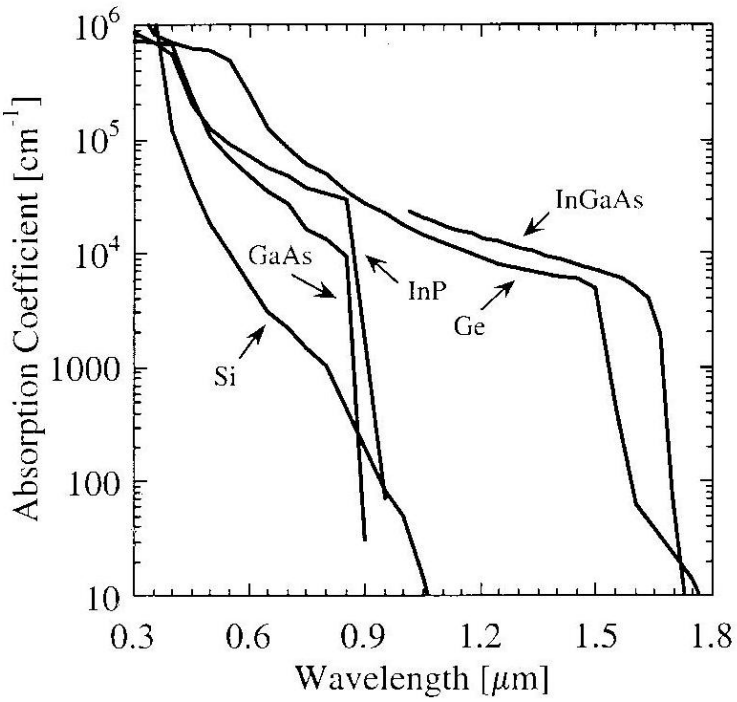

Figure 5.1: Optical absorption coefficient versus wavelength [14]

There are many desired characteristics that a photodetector needs to fulfil to be used for specific applications.

1. **Speed**: The photodetector needs to be able to respond to the incoming high-speed light data. For this, the generation of carriers should happen close to the metal contacts to reduce *transit times*. The electric potential in which they move should be strong enough to enable them to move at the saturation drift velocity. The capacitance of the device should be minimal too.

2. **Quantum efficiency**: Quantum efficiency is defined as the number of carriers produced per incident photon. An ideal process will produce an electron-hole pair for every incident photon. But, part of the light will be reflected or scattered, which results in wasted photons. Hence, design of the photodetectors tries to minimize the reflection losses. Further, if the active area of the photodetector is small compared to the incident light's spot size, a large part of the light is wasted. Thus,

another way to improve the quantum efficiency is to increase the active area.

3. **Low noise**: The noise determines the smallest signal that can be detected. It can come from various sources like (1) leakage current due to the applied bias in the absence of light (dark current), (2) thermal excitation of carriers, (3) shot noise from discrete random events of carrier generation or motion, and (4) low frequency 1/f noise.

There are trade-offs involved in optimization of these parameters. For example, decreasing the semiconductor absorption width can improve speed by reducing the transit time, but in turn decreases the quantum efficiency because some photons may pass through unabsorbed. Similarly, increasing the area of the photodetector improves quantum efficiency, but also increases the capacitance and limits its speed.

There are different types of photodetectors that may be better suited for different applications. Some of the main types are:

- Photoconductors
- Photodiodes
- Metal-semiconductor-metal photodetectors (MSM-PDs)

5.1 Principle of operation

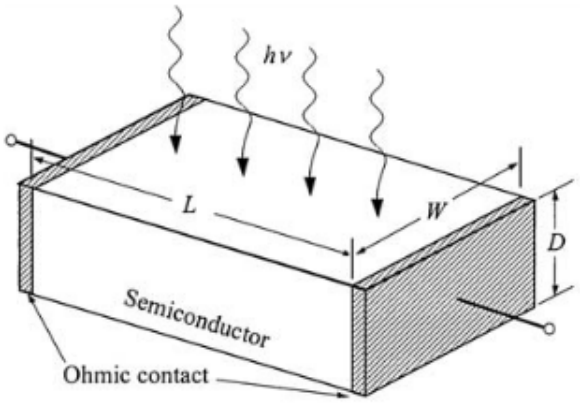

Figure 5.2: Schematic of a photoconductor [15]

Figure 5.2 shows the schematic of a typical photoconductor. When light is absorbed by the semiconductor, charge carriers are created. The carrier densities increase according to $n \rightarrow n + \Delta n$ and $p \rightarrow p + \Delta p$. This causes the conductivity of the material to change. Setting $\Delta n = \Delta p$, the photocurrent is given by $I_p = \Delta\sigma \mathbf{E} A = (\mu_n + \mu_p)\Delta n q \mathbf{E} A$. μ_n, μ_p are the carrier mobilities, $\mathbf{E}$ is the electric field and A is the active area. The photogenerated carrier density Δn is proportional to the optical power P_{opt} as given by $\Delta n = \frac{\eta(P_{opt}/h\nu)}{V}$, where η is the quantum efficiency, V is the active volume and $h\nu$ is the energy of one photon. So, the photocurrent is linearly proportional to the incident light power.

The structure of a MSM-PD is shown in Fig. 5.3. It consists of two semiconductor-metal Schottky barriers connected back-to-back. The metal

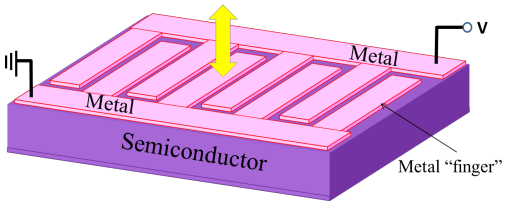

Figure 5.3: Schematic of a MSM-PD [16]

contacts are arranged in the form of interdigitated fingers for efficient light and charge collection. The depth of the active area is usually made slightly larger than the absorption length of light. For GaAs, it is close to 1 μm for wavelengths less than 0.87 μm. The doping is kept low because this enables formation of a better Schottky contact than in the highly doped case where contacts tend to become more ohmic. Figure 5.4 shows the band-diagram of a MSM-PD at equilibrium and for an applied bias. With the applied bias, one of the Schottky barriers will be forward biased and the other one will be reverse biased. The reverse bias increases the Schottky barrier for the electrons at the cathode, but the forward bias decreases the Schottky barriers for the holes at the anode. Therefore, the dark current is largely due to the thermally generated holes at the anode. The photogenerated electron-hole pairs travel to opposite electrodes as indicated.

MSM-PDs have good speed performance because there is a short transit time for the carriers, defined by the spacing between the metal electrodes. However, the area for light collection decreases as the gap decreases assuming a fixed size for the metal electrodes. Further, the RC-constant has also been

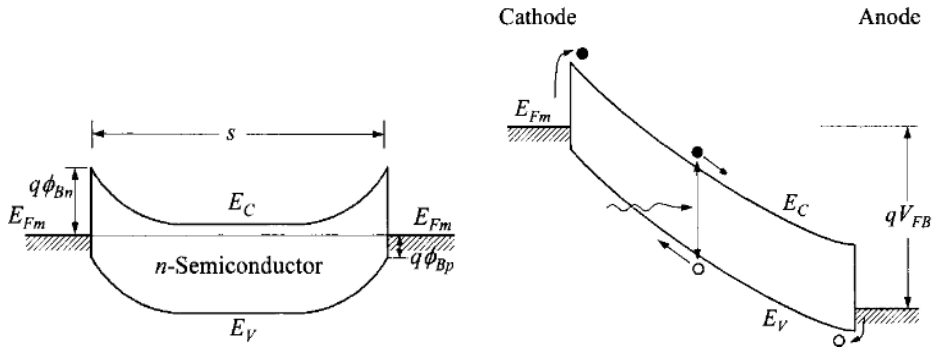

(a) At equilibrium (b) With applied bias

Figure 5.4: Band-diagram of a MSM-PD under different conditions [15]

shown to increase with decreasing spacing. Therefore, the finger spacing is a design parameter that needs to be optimized. Photodetectors with hundreds of GHz bandwidth have been realized.

Further, MSM-PDs have low capacitance because of the two-dimensional device structure. They also have the advantage of compatibility with field effect transistor (FET) processes because the fabrication is a simple planar process. The main disadvantages of MSM-PDs are their low responsivity and their dark current because of the low Schottky barrier for one type of carrier. There have been several designs to overcome it; for example, the use of a thin barrier-enhancement layer between the semiconductor and metal has suppressed the dark current by six orders of magnitude with respect to the photocurrent [17].

CHAPTER 6

FABRICATION OF INTEGRATED PARABOLIC REFLECTOR

With the intention of increasing the light-collecting efficiency of MSM-PDs, several designs have been proposed in the literature. Because nearly half of the light gets reflected off the metal contacts, transparent metals like indium tin oxide (ITO) and cadmium tin oxide (CTO) have been used [18, 19]. These metal contacts, however, have higher resistivity than the typical Schottky contacts like Ti/Pt/Au. ITO contacts can have resistivity of 10^{-3} Ω-cm, whereas the Ti/Au contacts can show 100-1000 times lower resistivity. Thus, the responsivity can be increased by a factor of two at the expense of a lower bandwidth due to larger RC time constants. Apart from this, MSM-PDs integrated with a resonant cavity of distributed Bragg reflectors (DBRs) have been fabricated to increase responsivity by re-using the light through multiple passes [20]. The disadvantage of the DBR is that the enhancement is wavelength specific and the attenuation may be detrimental for certain parts of the spectrum. As an alternate approach, we attempted to integrate

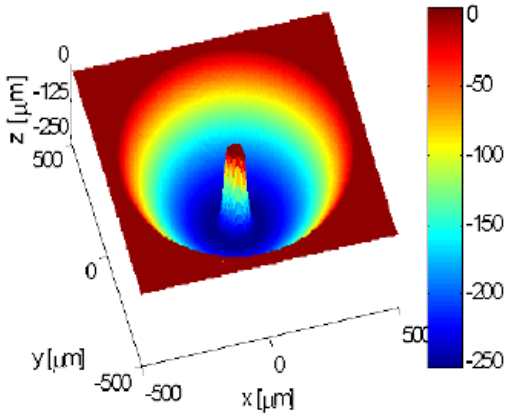

Figure 6.1: Schematic of the MSM-PD with integrated parabolic reflector

a parabolic reflector along with the MSM-PD to be able to collect more light. This is a geometric-type modification of the device only, and so it is

wavelength independent and moreover it can be used in conjunction with the material-type modifications like the transparent electrodes, for better performance. Figure 6.1 shows a schematic of the proposed device. It consists of a planar MSM-PD with a parabolic reflector underneath it to reveal a pedestal for the MSM-PD, positioned at the parabola's focus.

A small part of the incident light will directly illuminate the MSM-PD and cause a photocurrent. The rest of the light will reflect off the parabolic mirror and focus onto the MSM-PD. This will lead to a higher photocurrent, while still retaining its speed and capacitance intact. The diameter of the parabola can be as large as possible to collect more light, but the etch depth increases proportionately. Taking fabrication capabilities into consideration, we chose the diameter of the parabola to be $D = 1$ mm and, therefore, its depth to be 250 μm, following $y = \frac{x^2}{D}$. This particular parabola has its focal position at the top of the MSM PD pedestal.

6.1 Process steps

PC etching is used for etching the parabolic reflector after fabrication of the MSM-PD. The steps for the process are:

1. Photolithography of the MSM-PD: First, we did photolithography on the n-type GaAs substrate to define the MSM interdigitated fingers. We had three sizes of the fingers/spacing: 5 μm, 4 μm and 3 μm.

Table 6.1: Photolithography steps

Step	Positive resist	Negative resist
Spin photoresist (AZ5214)	0-1000 rpm (250 rpm/s) 10 s 1000-5000 rpm (1000 rpm/s) 30 s	Same
Soft-bake	1 min	50 s
Edge-bead removal	Yes	Yes
Exposure	1 min	30 s
Post-bake	–	1 min
Flood exposure	–	2 min
Development	45 s	30 s

Because the chrome pattern is dark, we needed to do lithography with a negative resist to define the desired reverse pattern. Table 6.1 lists the steps for lithography with positive and negative resists that we followed.

2. Metallization: Schottky contact on GaAs is generally done by depositing titanium (Ti) for adhesion promotion and Gold (Au). We deposited 5 nm of Ti followed by 100 nm of Au using the thermal evaporator (CHA). This was followed by lift-off in acetone to define the MSM fingers. Figure 6.2 shows a microscope image of the fabricated device.

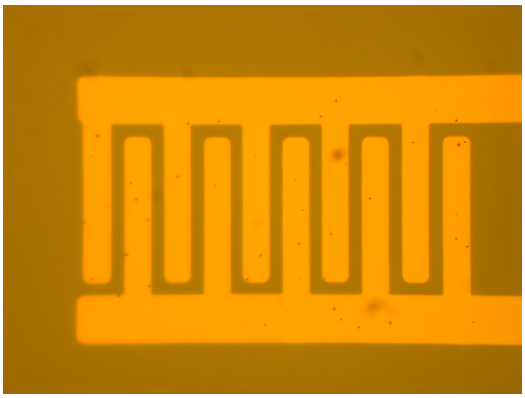

Figure 6.2: Microscope image of the MSM-PD with 5 μm finger width and spacing

3. Masking: As we had to etch 250 μm deep, we needed a high etch rate to keep the time practical. Although PC etching works even without any oxidizer in the etchant, its etch rate is less than 1 μm/min for maximum light intensity. Therefore, we added H_2O_2 into the etchant to get etch rates close to 4-5 μm/min. Adding the oxidizer makes the wet etch rate non-zero, which is problematic for the fabricated MSM device. Hence, we masked it prior to PC etching. We used 1 μm of Si_3N_4 followed by metal layers of 5 nm Cr - 50 nm Au - 5 nm of Cr. The mixed frequency Si_3N_4 provides mechanical stability without wrinkling when suspended and the metal layers reflect the light and prevent PC etching underneath.

4. Photolithography of the C-pattern: To be able to PC etch the parabola, we created a circular window opening with the MSM-PD at its center. Figure 6.3 shows a microscope image of the sample with the C-shaped circular window. There is a half-bridge which contains the leads of the MSM terminating in metal pads outside the circle. The process was similar to the first step.

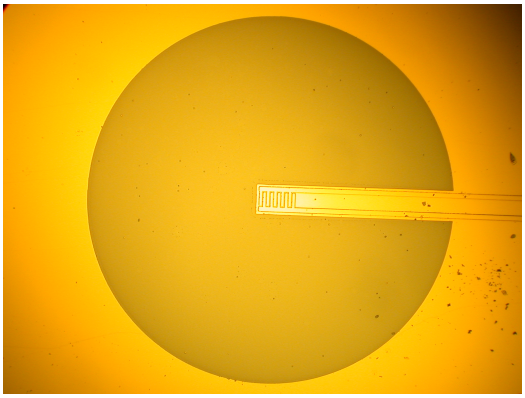

Figure 6.3: Microscope image of the masked sample with circular window open for PC etching

5. PC etching: To etch the parabolic reflector, we initially used a circular gradient pattern with a parabolic gradient. However, because the depth to which we etch is quite great, after a few minutes, the shape could not be maintained well. This happened because the gradient pattern would make the surface non-planar and different parts would be at different planes thereby going out of focus differently. To overcome this, we projected a solid white circle with its radius shrinking parabolically with time. In other words, we projected a movie of a parabolically contracting circle. This keeps the surface flat. The etchant used was 4:1:80 H_2SO_4:H_2O_2:H_2O. Various durations of time were attempted for the etching movie. It was seen that roughly 200 μm could be etched in 80 minutes.
6. Mask removal: To expose the MSM device, the metal and Si_3N_4 were removed by using HF. HF etches Si_3N_4, which then removes the masking metal too.

6.2 Results and discussion

6.2.1 Device testing steps

An important test for the performance of a photodetector is its current-voltage (IV) characteristics in the absence and presence of light. Ideally, no current should flow in the dark and a large current should flow when illuminated. Moreover, the current should increase linearly with the optical power. When no voltage is applied, there is no field created between the fin-

gers and no current flows. As the voltage increases above a threshold value, the photocurrent increases exponentially. But, practically, there is a finite dark current. Some possible mechanisms for the dark current are: (i) thermal generation of carriers, (ii) leakage current due to applied bias and (iii) crystallographic defect-generated carriers. Another important test for our device is the photodetector speed. This can be measured by modulating the light source at different frequencies and measuring the photocurrent amplitude. At high frequencies, the charge carriers cannot travel fast enough before the arrival of the next pulse of light, so the modulation amplitude of the photocurrent reduces. The frequency at which the photocurrent amplitude reduces to $1/\sqrt{2}$ of its DC value is called the 3 dB frequency or bandwidth of the photodetector. With these two tests, the device testing flow is shown in Fig. 6.4. With the higher light collection capacity, the photocurrent for

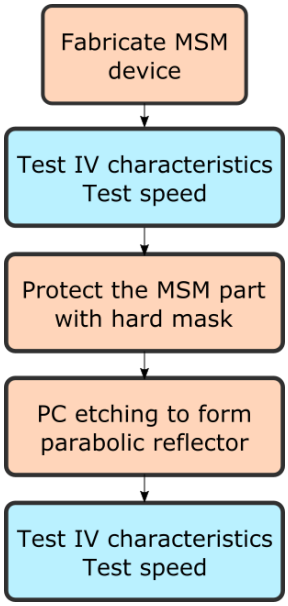

Figure 6.4: Flow diagram of the MSM-PD device testing

a given voltage should increase. Because the effective area of light collection has increased by about 100 times (0.1 mm $\times$ 0.1 mm is the MSM-PD areal dimension, 1.0 mm is the parabola's diameter), the current is also expected to increase by about 1-2 orders of magnitude, taking into account the imperfect reflections and mirror's surface roughness. The bandwidth, however, remains the same.

6.2.2 IV characteristics

Figure 6.5 shows the schematic of the setup used for measuring IV characteristics. There are two metal probe tips with x, y, and z motion control vacuumed onto a platform. The sample is placed on a stage with x, y, and z motion control. There is a microscope for viewing the sample and probe tips. The probe tips are roughly brought into the vicinity of the metal pads of the MSM-PD by adjusting the x and y knobs connected to them. For finer adjustments, the sample is moved by looking through the microscope. Finally, each probe tip is lowered to touch the metal pad by adjusting the z knob. The way to make sure that the probe is in fact touching the metal pad is to go down until the probe slides over the sample, scraping it a little. Any one of the probe tips (polarity does not matter in the MSM-PD),

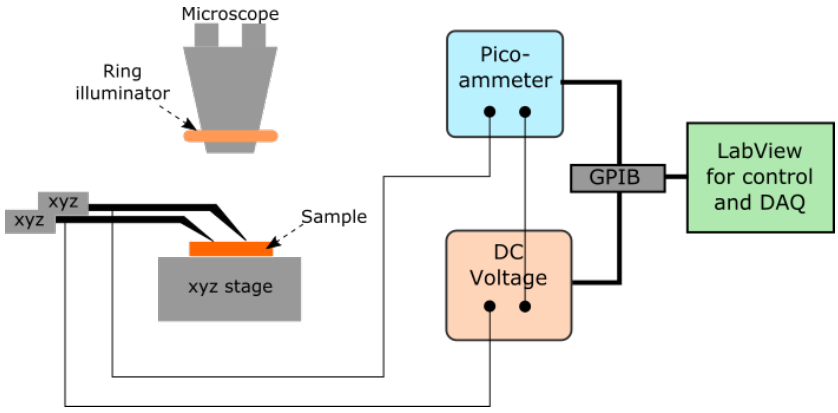

Figure 6.5: Schematic of the IV testing setup

is connected to the positive of a DC voltage source. We used the Keithley 33250A function generator in the DC setting to act as a DC voltage source. The ground of the voltage source is connected in series to a Keithley 6485 picoammeter. The other probe tip is connected to the picoammeter to complete the circuit. The illumination source is simply the ring illuminator of the microscope. The experiment is automated using LabView, by control of the instruments and data acquisition (DAQ) using GPIB-interface. Cyclically, the DC voltage is set at a value and the current reading is acquired. In this way, the voltage is swept from an initial to a final value defined by the user, and the corresponding currents are read and stored.

Figure 6.6 shows the IV-characteristics of one of the several MSM-PDs fabricated. They were fabricated on n+-type GaAs with Ti/Au Schottky

contacts. The finger widths and spacing vary from 3 to 5 μm.

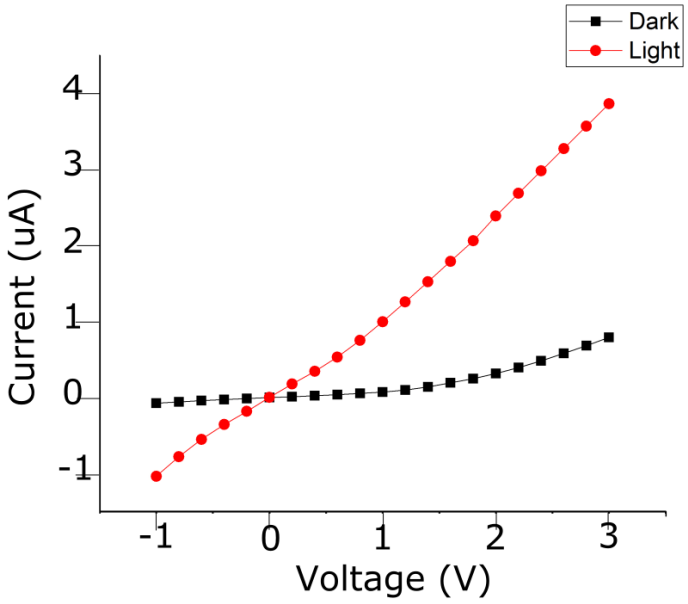

Figure 6.6: IV characteristics of an MSM-PD with 5 μm finger widths and spacing

The IV-characteristics show a significant dark current in the range of a few μA. Although there is a definite increase in current in the presence of light, the dark current is too large for practical purposes. One possible explanation for this observed dark current is that the devices were fabricated directly on the substrate material and not on a epitaxial layer. Generally substrate material is poor quality and is not used for actual device-grade applications. Another reason for the large dark current could be that the Schottky contacts have a small barrier because of the high doping level in the GaAs. Generally, semi-insulating material is preferred for making Schottky contacts as it forms a higher barrier. Despite these difficulties, clear photodetection is observed. The responsivity was estimated to be close to 0.1 A/W.

6.2.3 Parabolic PC etching

Next, the samples were protected with a hard mask and patterned as described in section 6.1. Figure 6.3 shows a microscope image of the sample prior to PC etching, after the masking and patterning. As described, we carried out PC etching using an 80-minute movie of a shrinking white circle

projected to overlap with the circular window on the sample. Figure 6.7 shows a cleaved cross section SEM image of one of the samples.

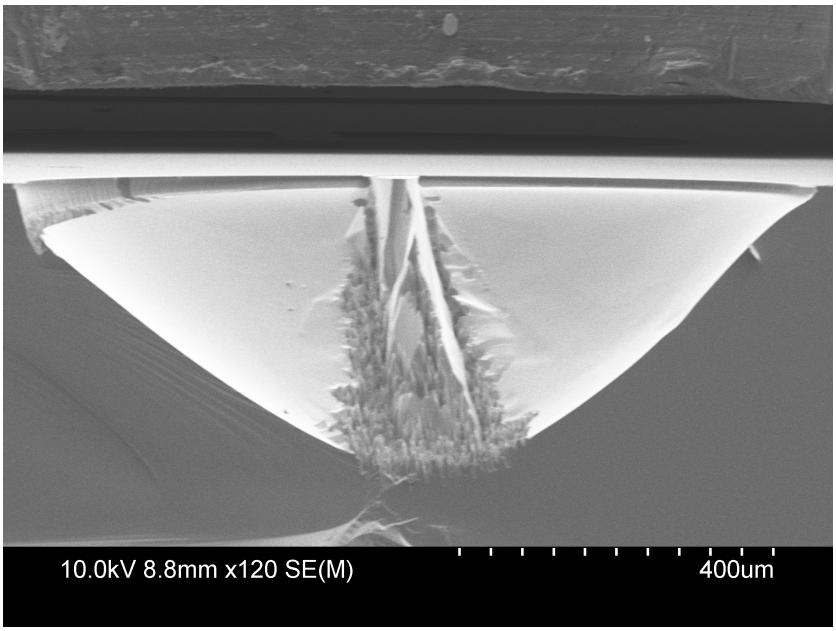

Figure 6.7: Cross-section SEM of a device after PC etching

Due to the high wet etch rate of the etchant (even without light), the half-bridge gets severely undercut because of the long duration of etch. However, the parabolic profile can be achieved nearly perfectly as shown in the fit in Fig. 6.8. This was done by etching on a plain substrate with 2:2:100 HCl:H_2O_2:H_2O for 1.5 hours.

6.2.4 Subsequent steps

We could not run the full sequence of tests because of the severe undercut issue. Consequently, we need to make some modifications in the process flow.

1. To reduce the wet etch rate, we can reduce or remove the H_2O_2 from the etchant and do very long PC etches to get to the desired depth without undercut.

2. To protect the devices, we can change the mask design to have wider bridges so that the MSM-PD is masked even with some undercut during etching.

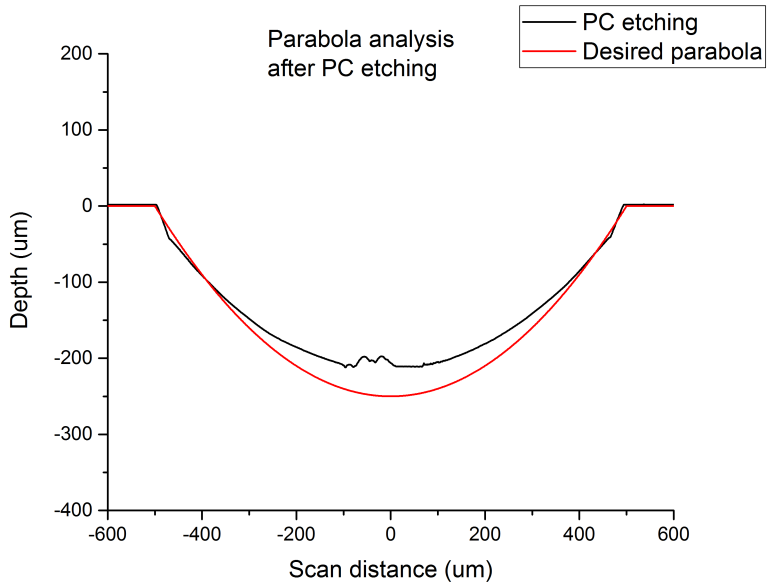

Figure 6.8: Optical profiler scan of a parabolic etch along with the desired profile

3. To improve the quality of devices, we can use a 1 μm thick semi-insulating epitaxial layer on top of the n-type GaAs. This will enable better Schottky contacts (and hence lower dark current) while still retaining fast PC etching below the semi-insulating layer.

CHAPTER 7

CONCLUSIONS AND FUTURE DIRECTIONS

7.1 PC etching for device fabrication

Based on the grayscale etching property of PC etching, it is possible to integrate this process into conventional microfabrication to enhance our device fabrication capability. This was demonstrated in the case of the MSM-PD. However, there are some limitations to the process in terms of which kinds of materials and doping can be used for PC etching. With simple PC etching, it is not possible to etch p-type III-V materials due to the unfavorable band-bending. Some possible solutions to this can be to apply a potential between the semiconductor and electrolyte to bend the bands upward or to use UV light to create hot holes close to the surface [7]. Despite this limitation, there are a lot of possibilities for applications with the materials which we can PC etch. Angled mirrors, apodized gratings and microlenses are some photonic applications in which PC etching can be used. A vertically adiabatic tapered waveguide is another major application of PC etching that makes use of the unique grayscale etching capability. The tapered waveguide can be used to shift the optical mode from a waveguide in one plane to one in a different plane. We are looking to implement active-passive monolithic integration by this technique.

Another limitation of the current PC etching setup is its resolution. A pixel on the PowerPoint screen corresponds to nearly 10.5 μm on the sample plane. This makes it impossible to etch smaller feature sizes. Therefore, improving the demagnification ratio of the 4f-imaging system is needed, to create a scaling of about 1 pixel = 1 μm, even if it is not diffraction-limited. A higher NA objective lens will be used for this purpose. A scanning optical fiber setup can also be implemented to etch sub-micron features. Further, because the image is digitally projected, pixellation could be a possible issue

for small features. Currently, we overcome this problem by applying circular xy motion of the stage to blur the pixels. In the future, we will look into using a laser as the light source along with a spatial light modulator to project smooth images.

7.2 Fundamental studies on PC etching

There are several aspects of PC etching that are not well understood. The formation of defect structures during PC etching in some regimes needs more careful study and cross-validation by other techniques such as TEM. The cause and mechanism of the formation of octahedral-like structures are highly unclear. We would need to do a systematic study of the stages through which the structures form to be able to understand them. These structures could then possibly be used for applications such as an array of scatterers. The characteristics of diffusion-limited PC etching also present some very interesting directions, such as spatially varying concentration gradients and etch sinks.

Anisotropic PC etching shows promise to solve the problem of vertical wet etching. The chemical formulation needs more refinement to narrow down parameters to the best regime for anisotropic PC etching.

PC etching, therefore, presents a whole new field of study by integrating semiconductor properties with wet etching. It creates a possibility of fabrication of unconventional devices not possible through regular microfabrication. Moreover, the PC etching process in itself has many interesting properties that make it worth pursuing for fundamental research.

REFERENCES

[1] K. Totsu, K. Fujishiro, S. Tanaka, and M. Esashi, "Fabrication of three-dimensional microstructure using maskless gray-scale lithography," *Sensors and Actuators A: Physical*, vol. 130, pp. 387–392, 2006.

[2] C. Xia and N. Fang, "Fully three-dimensional microfabrication with a grayscale polymeric self-sacrificial structure," *Journal of Micromechanics and Microengineering*, vol. 19, no. 11, p. 115029, 2009.

[3] J. Kim, D. Joy, and S.-Y. Lee, "Controlling resist thickness and etch depth for fabrication of 3D structures in electron-beam grayscale lithography," *Microelectronic Engineering*, vol. 84, no. 12, pp. 2859–2864, 2007.

[4] P. A. Kohl, "Photoelectrochemical etching of semiconductors," *IBM Journal of Research and Development*, vol. 42, no. 5, pp. 629–638, 1998.

[5] F. Ostermayer Jr, P. Kohl, and R. Lum, "Hole transport equation analysis of photoelectrochemical etching resolution," *Journal of Applied Physics*, vol. 58, no. 11, pp. 4390–4396, 1985.

[6] T. D. Lowes and D. T. Cassidy, "Photochemical etching of n-InP as a function of temperature and illumination," *Journal of Applied Physics*, vol. 68, no. 2, pp. 814–819, 1990.

[7] D. Podlesnik, H. Gilgen, and R. Osgood Jr, "Deep-ultraviolet induced wet etching of GaAs," *Applied Physics Letters*, vol. 45, no. 5, pp. 563–565, 1984.

[8] F. Ostermayer Jr and P. Kohl, "Photoelectrochemical etching of p-GaAs," *Applied Physics Letters*, vol. 39, no. 1, pp. 76–78, 1981.

[9] R. Khare and E. L. Hu, "Dopant selective photoelectrochemical etching of GaAs homostructures," *Journal of The Electrochemical Society*, vol. 138, no. 5, pp. 1516–1519, 1991.

[10] C. Youtsey, I. Adesida, and G. Bulman, "Highly anisotropic photoenhanced wet etching of n-type GaN," *Applied Physics Letters*, vol. 71, no. 15, pp. 2151–2153, 1997.

[11] C. Youtsey, L. Romano, and I. Adesida, "Gallium nitride whiskers formed by selective photoenhanced wet etching of dislocations," *Applied Physics Letters*, vol. 73, no. 6, pp. 797–799, 1998.

[12] M. Abrahams and C. Buiocchi, "Etching of dislocations on the low-index faces of GaAs," *Journal of Applied Physics*, vol. 36, no. 9, pp. 2855–2863, 1965.

[13] A. Bruzzone and A. Reverberi, "An experimental evaluation of an etching simulation model for photochemical machining," *CIRP Annals-Manufacturing Technology*, vol. 59, no. 1, pp. 255–258, 2010.

[14] E. D. Palik, *Handbook of Optical Constants of Solids*. Academic Press, 1998, vol. 3.

[15] S. M. Sze and K. K. Ng, *Physics of Semiconductor Devices*. John Wiley & Sons, 2006.

[16] N. Das, F. Fadakar Masouleh, and H. R. Mashayekhi, "A comprehensive analysis of plasmonics-based GaAs msm-photodetector for high bandwidth-product responsivity," *Advances in OptoElectronics*, vol. 2013, 2013.

[17] L. Sang, M. Liao, Y. Koide, and M. Sumiya, "High-performance metal-semiconductor-metal InGaN photodetectors using CaF_2 as the insulator," *Applied Physics Letters*, vol. 98, no. 10, p. 103502, 2011.

[18] J.-W. Seo, A. A. Ketterson, D. G. Ballegeer, K.-Y. Cheng, I. Adesida, X. Li, and T. Gessert, "A comparative study of metal-semiconductor-metal photodetectors on GaAs with indium-tin-oxide and ti/au electrodes," *IEEE Photonics Technology Letters*, vol. 4, no. 8, pp. 888–890, 1992.

[19] W. Gao, P. R. Berger, G. J. Zydzik, H. M. O'Bryan, D. L. Sivco, and A. Y. Cho, "$In_{0.53}Ga_{0.47}As$ MSM photodiodes with transparent CTO Schottky contacts and digital superlattice grading," *IEEE Transactions on Electron Devices*, vol. 44, no. 12, pp. 2174–2179, 1997.

[20] K. Kishino, M. S. Unlu, J.-I. Chyi, J. Reed, L. Arsenault, and H. Morkoc, "Resonant cavity-enhanced (RCE) photodetectors," *IEEE Journal of Quantum Electronics*, vol. 27, no. 8, pp. 2025–2034, 1991.